FEA-Assisted Experimental Parameter Map Identification of Induction Motor for Wide-Range Field-Oriented Control

Jiwon Yoo, *Member, IEEE*, Joon-Hee Lee, *Member, IEEE*, and Seung-Ki Sul, *Fellow, IEEE*

***Abstract*—This article introduces an experimental parameter identification method for induction motor (IM) drives, aiming to accurately identify the motor parameters while considering magnetic saturation throughout the entire operating point. To address the rank-deficiency problem in experimental parameter identification for IMs, this article proposes a solution by constructing a stator inductance lookup table (LUT) with the assistance of finite element analysis. By conducting experimental tests, the leakage inductance and the rotor resistance are calculated across the entire operating range. To utilize the obtained parameter set for flux estimation in field-oriented control, the actual *dq*-axis current vector, which serves as the input domain of the parameter LUTs, is calculated through postprocessing. The accuracy of the proposed parameter LUTs is validated with the experimental results, demonstrating that the constructed parameter LUTs are suitable for a wide range of field-oriented control applications in electric vehicle traction motors.**

***Index Terms*—Electric vehicle (EV) traction motor, finite element analysis (FEA), induction motor (IM), offline commissioning, parameter identification.**

I. Introduction

As THE electric vehicle (EV) industry matures, traction motor drives for EV applications have become one of the most important applications for electric motor drives. In the automotive industry, permanent-magnet synchronous motors (PMSMs) have been widely used as the main traction motors, thanks to their high efficiency and high power density. However, the unquenchable residual flux of the permanent magnet consistently causes iron loss, which makes PMSMs less attractive in the auxiliary traction motor where the coasting mode is required. Instead of installing a clutch, the induction motor (IM) is emerging as an auxiliary traction motor, thanks to its capability of extinguishing the magnetic excitation and saving iron loss of the motor.

To adopt IM in the automotive traction motor, the energy-efficient operation is required. Moreover, the rotor flux excitation level needs to be carefully managed in automotive IM drives. Thus, the automotive IM should be operated with variable flux control, unlike the most of industrial drives that excite the rotor flux at a constant level for ease of control [1].

The variable flux operation of IM encounters various challenges in practical implementation. Most of all, since the magnetic saturation of the core varies according to the flux level, the motor parameters in the IM drive should be adequately identified according to the operating point [2]. Moreover, unlike PMSM drives that use vector control based on the measured rotor position, the field-oriented control (FOC) of IM relies on the rotor flux position estimated by a flux observer. As a result, any discrepancy between the actual motor parameters and the preset parameters in the flux observer can deteriorate stability and cause errors in field orientation. Therefore, it is crucial to identify the motor parameter variation across the entire operating range for automotive IM drives.

However, since the main application of IM drives has been the general-purpose IM drive, the studies on IM have focused on the nominal parameter commissioning at free- or locked-shaft conditions [3], [4]. Monjo et al. [5] proposed a test procedure to find the rated parameters of IM under locked-rotor conditions. In [6], the motor parameters considering iron loss were identified using the Heyland diagram under the rated load condition. These methods may be useful to identify the parameters of the industrial IMs, which are installed in the load application. However, as aforementioned, the nominal motor parameters would not be enough for accurate torque control under the variable flux control.

Recently, thanks to the development of the EV industry, many researchers are studying the motor parameter map identification across the entire operating points considering the magnetic saturation, especially for the PMSMs. Chen et al. [7] presented a dynamic motor model of the PMSM that accurately describes the magnetic saturation. The PMSM model in [7] is constructed based on stator flux lookup tables (LUTs), which are calculated through finite element analysis (FEA). Regarding experimental

Manuscript received 30 March 2023; revised 12 August 2023; accepted 9 October 2023. Date of publication 18 October 2023; date of current version 6 December 2023. This work was supported in part by the Korea Institute of Energy Technology Evaluation and Planning, Korea Government (MOTIE), under Grant 20225500000060 (Operation System for AC/DC Hybrid Distribution Network). Recommended for publication by Associate Editor M. Su. *(Corresponding author: Joon-Hee Lee.)*

Jiwon Yoo is with the Department of Smart Mobility Engineering, Inha University, Incheon 21999, South Korea (e-mail: jwyoo@inha.ac.kr).

Joon-Hee Lee is with the Department of Energy Engineering, Korea Institute of Energy Technology (KENTECH), Naju 58330, South Korea (e-mail: joonhee.lee@kentech.ac.kr).

Seung-Ki Sul is with the Department of Electrical and Computer Engineering, Seoul National University, Seoul 08826, South Korea (e-mail: sulsk@snu.ac.kr).

Color versions of one or more figures in this article are available at https://doi.org/10.1109/TPEL.2023.3325535.

Digital Object Identifier 10.1109/TPEL.2023.3325535

parameter commissioning, the authors in [8] and [9] investigated test procedures to extract the accurate motor parameter LUT. In [8], the fundamental stator flux vectors in the whole operating range are extracted through voltage information. Furthermore, Lee et al. [9] presented a parameter identification method including the effects of the spatial harmonics.

While there are many decent research works on parameter LUT identification for PMSMs, there is a lack of literature related to IM drives. The task of parameter LUT identification for IM is more challenging compared to that for PMSM due to the additional dynamic model in the rotor circuit. Furthermore, to construct the LUT, the accurate operating points should be decided first, which are the inputs of parameter LUTs. However, these operating points are determined by parameters of IM, so there is a contradiction in parameter map identification, which needs to be addressed.

Some researchers have been investigating on describing the dynamics of IM in a wide operating range. Since it is not easy to estimate the IM motor parameters experimentally, FEA is often adopted. Lee et al. [10] constructed a high-fidelity IM simulation model based on FEA. The motor parameters in the whole operating range are calculated by FEA, and five 5-D LUTs are constructed to describe the IM motor model. The simulation model in [10] can consider the various nonlinear dynamics of IM, such as magnetic saturation due to stator and rotor currents and slotting effects. However, since it requires not only stator current excitation but also rotor current manipulation to build 5-D LUT, it is not easy to apply it to the experimental parameter identification. Similarly, Lin et al. [11] proposed an FEA procedure to extract the reduced model parameters of IMs by dividing the skin effect and the magnetic saturation. However, the discrepancy between the FEA model and the actual motor should be addressed in the FEA-based methods in [10] and [11]. Kullick and Hackl [12] built a nonlinear machine model based on the steady-state stator flux map. The steady-state performance, such as efficiency, can be experimentally evaluated based on the proposed stator flux map. However, since the stator flux is selected for the machine parameter, the transient dynamics of the rotor circuit are not fully considered.

This article presents a parameter LUT identification of IMs, enabling FOC of IM based on the obtained parameter LUTs. Prior to the parameter LUT generation, this article introduces the rank-deficiency problem of IM parameter identification, which occurs in the parameter identification of IM in the experiments. To define whole motor parameters in an operating point, one of the motor parameters should be preset to shed the rank-deficiency. In this article, FEA is employed to preset the stator inductance L_s parameter LUT. However, due to the inevitable discrepancy between FEA and the actual motor, the L_s map obtained from FEA is adjusted with experimental results at no-load conditions. This adjustment of FEA data enables the derivation of a rational L_s LUT.

Based on the preset L_s LUT and the experimental results at various operating points, leakage inductance σL_s, mutual inductance L_m, and rotor resistance R_r are calculated. Each parameter set is calculated based on its own experimental results only, and it does not refer to the test results at other operating points. Therefore, an accurate parameter set can be obtained without any unproven assumptions.

Meanwhile, the inaccessibility of the actual rotor flux position makes conducting experimental tests with direct field-oriented control (DFOC) challenging. To address this issue, the proposed method collects the stator voltage information at various stator current magnitudes and slip frequencies. From each data point collected, the motor parameters and the rotor flux position are calculated. This approach allows for the accurate calculation of *dq*-axis current based on the estimated rotor flux position. Consequently, the parameter LUT with a uniform input grid of *dq*-axis current can be constructed by the postprocessing of the collected data.

The main contributions of this article can be summarized as follows.

1) The rank-deficiency problem in IM parameter identification is addressed by adopting FEA along with experimental results.
2) IM parameter calculation method independent to the coordinate system is presented.
3) Parameter LUTs with a uniform input grid of *dq*-axis current are constructed based on a recalculation method, ensuring accurate determination of the *dq*-axis current vector from the collected stator flux information.
4) The voltage reconstruction method is proposed to experimentally verify the obtained parameter LUTs.

In addition to the previously presented conference paper [13], this article provides the following.

1) Detailed process of the proposed parameter identification.
2) FOC implementation based on the proposed LUTs.
3) Experimental results under various operating conditions.

II. Rank-Deficiency Problem in Experimental Parameter Identification of Induction Motor

The stator voltage equation of IM can be expressed as follows:

$$\mathbf{v}_{\mathbf{dqs}}^{\boldsymbol{\omega}} = R_s \mathbf{i}_{\mathbf{dqs}}^{\boldsymbol{\omega}} + \omega_e \mathbf{J} \boldsymbol{\lambda}_{\mathbf{dqs}}^{\boldsymbol{\omega}} + \frac{d}{dt} \boldsymbol{\lambda}_{\mathbf{dqs}}^{\boldsymbol{\omega}} \tag{1}$$

where R_s and ω_e stand for the stator resistance and the synchronous speed, respectively. $\mathbf{v}_{\mathbf{dqs}}^{\boldsymbol{\omega}}$, $\mathbf{i}_{\mathbf{dqs}}^{\boldsymbol{\omega}}$, and $\boldsymbol{\lambda}_{\mathbf{dqs}}^{\boldsymbol{\omega}}$ denote the stator voltage, current, and stator flux vector, respectively. The superscript "ω" stands for the arbitrary synchronous reference frame rotating with speed, ω_e. In (1), $\mathbf{J}$ is the 90° rotation matrix, i.e.,

$$\mathbf{J} = \begin{bmatrix} 0 & -1 \\ 1 & 0 \end{bmatrix}. \tag{2}$$

The rotor equation of IM can be written as follows:

$$0 = R_r \mathbf{i}_{\mathbf{dqr}}^{\boldsymbol{\omega}} + \omega_{sl} \mathbf{J} \boldsymbol{\lambda}_{\mathbf{dqr}}^{\boldsymbol{\omega}} + \frac{d}{dt} \boldsymbol{\lambda}_{\mathbf{dqr}}^{\boldsymbol{\omega}} \tag{3}$$

where ω_{sl} is the slip frequency. $\mathbf{i}_{\mathbf{dqr}}^{\boldsymbol{\omega}}$ and $\boldsymbol{\lambda}_{\mathbf{dqr}}^{\boldsymbol{\omega}}$ denote the rotor current and the rotor flux vector, respectively.

The IM dynamics in (1) and (3) can be represented with the circuit diagram in Fig. 1. The relation between $\boldsymbol{\lambda}_{\mathbf{dqr}}^{\boldsymbol{\omega}}$ and $\mathbf{i}_{\mathbf{dqr}}^{\boldsymbol{\omega}}$ can be formulated as

$$\boldsymbol{\lambda}_{\mathbf{dqr}}^{\boldsymbol{\omega}} = L_m \left(\mathbf{i}_{\mathbf{dqs}}^{\boldsymbol{\omega}} + \mathbf{i}_{\mathbf{dqr}}^{\boldsymbol{\omega}} \right). \tag{4}$$

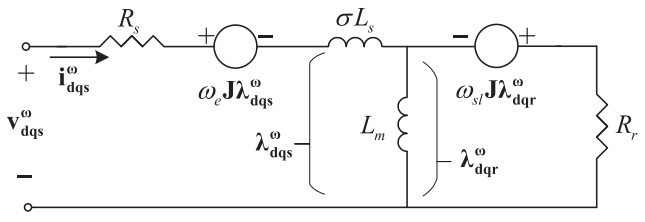

Fig. 1. Inverse-Γ model of IM.

From (4), (3) can be rewritten as follows:

$$R_r \mathbf{i}^{\omega}_{\mathbf{dqs}} = \left(\frac{R_r}{L_m} + \omega_{sl} \mathbf{J} \right) \boldsymbol{\lambda}^{\omega}_{\mathbf{dqr}} + \frac{d}{dt} \boldsymbol{\lambda}^{\omega}_{\mathbf{dqr}}. \tag{5}$$

The relation between $\boldsymbol{\lambda}^{\omega}_{\mathbf{dqs}}$ and $\boldsymbol{\lambda}^{\omega}_{\mathbf{dqr}}$ can be expressed as

$$\boldsymbol{\lambda}^{\omega}_{\mathbf{dqs}} = \boldsymbol{\lambda}^{\omega}_{\mathbf{dqr}} + \sigma L_s \mathbf{i}^{\omega}_{\mathbf{dqs}}. \tag{6}$$

Regarding the parameter identification, the derivative terms in (1) and (5) should be carefully managed. If a high-frequency signal is injected to exploit the derivative terms, various nonlinear effects, such as skin effect of the rotor bars and partial magnetic saturation of the core would interfere with the accurate parameter identification. Therefore, in this article, the steady state of (1) and (5) is only considered in the parameter identification as follows:

$$\mathbf{v}^{\omega}_{\mathbf{dqs}} = R_s \mathbf{i}^{\omega}_{\mathbf{dqs}} + \omega_e \mathbf{J} \boldsymbol{\lambda}^{\omega}_{\mathbf{dqs}} \tag{7}$$

$$R_r \mathbf{i}^{\omega}_{\mathbf{dqs}} = \left(\frac{R_r}{L_m} + \omega_{sl} \mathbf{J} \right) \boldsymbol{\lambda}^{\omega}_{\mathbf{dqr}}. \tag{8}$$

Therefore, (6)–(8) are the fundamental equations describing the IM dynamics. Since they are vector equations, each equation consists of two scalar equations. Thus, (6)–(8) can be treated as six independent equations. However, the number of the unknown variables in (6)–(8) are eight, i.e., R_s, R_r, σL_s, L_m, λ^{ω}_{ds}, λ^{ω}_{qs}, λ^{ω}_{dr}, and λ^{ω}_{qr}. These eight unknown variables tend to vary according to the operating point. For example, σL_s and L_m change due to the magnetic saturation, and the flux vectors also vary according to the current variation. Furthermore, the inverse-Γ model is not the real physical model of IM, but an equivalent circuit with the minimum number of motor parameters, i.e., stator and rotor leakage inductances are unified with σL_s. Similarly, R_r in the inverse-Γ model is not an actual rotor resistance but an equivalent resistance referred to the stator side. Thus, it also varies according to the operating point. Therefore, simultaneously solving the equations at different operating points would lead to erroneous results.

The unique parameter expected to be constant regardless of the operating points is R_s. Of course, R_s may change with the operating point due to temperature variation and skin effect. However, this article assumes that the stator temperature is measured accurately through the temperature sensor installed at the stator, and the R_s variation due to the skin effect could be negligible from the fundamental component point of view. Therefore, R_s can be measured by offline commissioning, such as dc injection tests [14], [15].

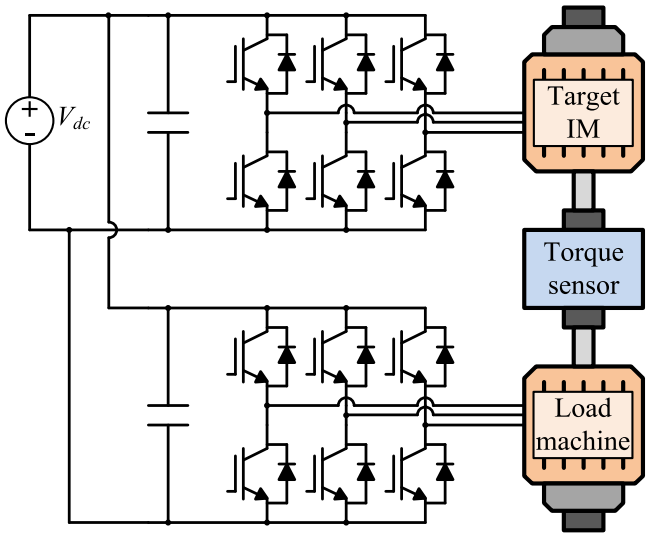

Fig. 2. Test bench setup.

Nevertheless, the number of the given equations is six, and the unknown variables are still seven. Therefore, there is a rank deficiency to solve the equations. To solve this rank-deficient problem, at least a parameter should be identified through an additional method. In this article, the FEA-assisted parameter LUT identification method will be introduced.

III. Proposed Parameter Identification Method

A. Test Bench Configuration

The proposed parameter identification method focuses on accurate parameter measurement at the entire operating region. Therefore, instead of the parameter commissioning at locked- or free-shaft conditions, a motor-generator set that can set the speed and load conditions independently is selected for the test bench configuration, as shown in Fig. 2. The target IM and the load machine are connected to the voltage source inverters that share the dc link. The target IM is controlled under the current regulation mode, while the load machine regulates the rotor speed. The shaft resolver measures accurate mechanical speed. Therefore, the slip frequency of the target IM can be regulated accurately without knowing the proper motor parameters. In this paper, a 90 kW-rated automotive-grade IM was selected as the target motor. Fig. 3(a) and (b) shows the motors and inverters used in the experimental verification.

B. Stator Inductance Identification at No-Load Condition

The stator inductance L_s can be defined as follows in Fig. 1:

$$L_s = L_m + \sigma L_s. \tag{9}$$

At the null slip frequency, (9) can be rewritten as

$$\mathbf{v}^{\omega}_{\mathbf{dqs}} = R_s \mathbf{i}^{\omega}_{\mathbf{dqs}} + \omega_e \mathbf{J} L_s \mathbf{i}^{\omega}_{\mathbf{dqs}}. \tag{10}$$

Thus, L_s at no-load condition can be calculated as

$$L_{s,\mathrm{EXP}} \left(||\mathbf{i}^{\omega}_{\mathbf{dqs}}|| \right) = \frac{||\mathbf{v}^{\omega}_{\mathbf{dqs}} - R_s \mathbf{i}^{\omega}_{\mathbf{dqs}}||}{\omega_e ||\mathbf{i}^{\omega}_{\mathbf{dqs}}||}. \tag{11}$$

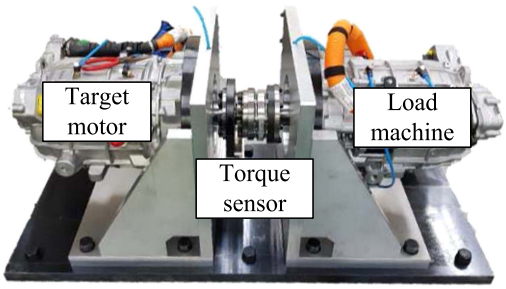

(a)

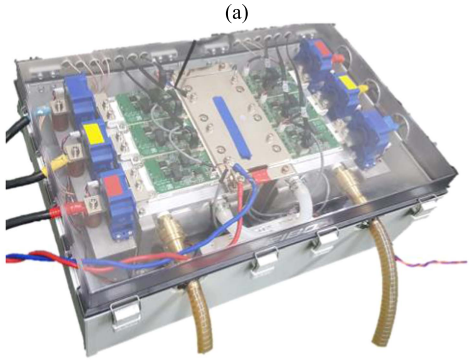

(b)

Fig. 3. (a) Motor-generator set. (b) Inverters.

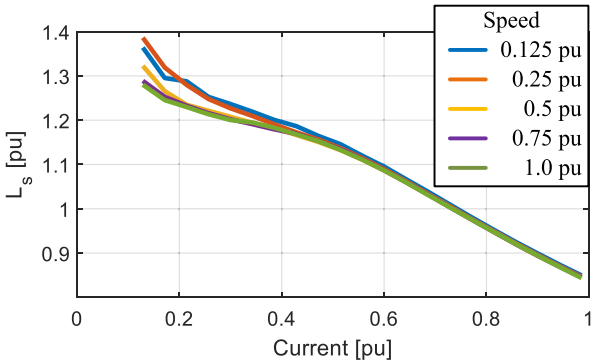

Fig. 4. Estimated stator inductance at no-load condition.

$L_{s,\mathrm{EXP}}(I_{s0})$ represents the experimentally calculated stator inductance where the stator current magnitude is I_{s0} and $\omega_{sl} = 0$. Since ω_{sl} is regulated to null, ω_e in (11) can be replaced with the rotor speed ω_r, measured by the position sensor.

To achieve high accuracy in $L_{s,\mathrm{EXP}}$, the rotor speed should not be regulated to too low speed, where the inverter nonlinearity or small R_s error can deteriorate the calculation accuracy. Also, to reduce the effect of the iron loss, the L_s estimation should not be conducted at too high speed. In addition, the sweep range of I_{s0} at too high speed would be limited by the dc-link voltage. Fig. 4 shows the estimated L_s of the target IM. Before identifying L_s, the inverter nonlinearity has been measured offline as shown in Fig. 5, and it has been compensated during the L_s measurement [15]. Despite the inverter nonlinearity compensation, it can be noticed that the estimated inductance at low speeds and small I_{s0} deviates from the trend curve. Regarding these constraints, half of the base speed has been selected for the test speed of the L_s estimation. In this article, all the parameters and the current are denoted as per-unit values. The unit value of the inductance refers to the nominal stator inductance. The unit value of the current refers to the rated current magnitude. It can be observed that L_s is conspicuously saturated, as the motor current increases.

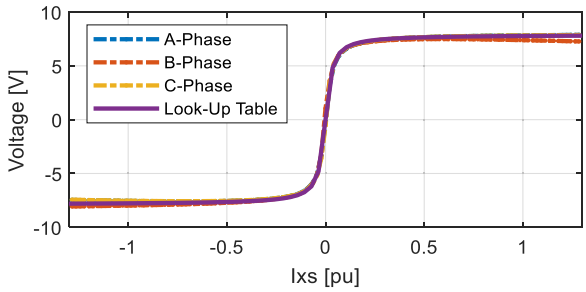

Fig. 5. Inverter nonlinearity effect and compensation table.

C. Estimation of Stator Inductance at Loaded Conditions Based on FEA Results

The L_s measurement in the previous section has the limitation that the test should be conducted at the null slip frequency. Therefore, L_s at the loaded condition is hard to be estimated. Instead, the FEA can be utilized in order to infer the magnetic saturation of L_s at the loaded condition. Among various ways to calculate L_s using FEA, the method in [10] is used in this article. The FEA is conducted by Ansys Maxwell software, and the stator winding is excited by the current in the FEA. The L_s is identified by the simulation model based on the FEA results while changing the slip frequency ω_{sl} and current magnitude I_s. In other words, the dq-axes currents are set as follows, assuming the indirect field-oriented control (IFOC) with a constant preset rotor time constant $\tau_{r0} = L_{m0}/R_{r0}$

$$i_{ds}^{\hat{e}} = \frac{I_s}{\sqrt{1+\tau_{r0}^2\omega_{sl}^2}} \tag{12}$$

$$i_{qs}^{\hat{e}} = \sqrt{I_s^2 - {i_{ds}^{\hat{e}}}^2} \tag{13}$$

where the superscript $\hat{e}$ denotes the estimated rotor flux reference frame in the IFOC. The preset rotor time constant can be determined by offline commissioning such as the free-run test [16].

Unlike the experimental tests where only the stator voltage and current can be monitored, the FEA can provide more information in the IM model: the rotor flux position. Since the rotor flux can be observed in FEA, L_s can be calculated as follows at the steady state:

$$L_{s,\mathrm{FEA}}\left(i_{ds}^{\hat{e}}, i_{qs}^{\hat{e}}\right) = \frac{\boldsymbol{\lambda}_{\mathbf{dqs}}^{\hat{\mathbf{e}}\,\mathbf{T}}\boldsymbol{\lambda}_{\mathbf{dqr}}^{\hat{\mathbf{e}}}}{\mathbf{i}_{\mathbf{dqs}}^{\hat{\mathbf{e}}\,\mathbf{T}}\boldsymbol{\lambda}_{\mathbf{dqr}}^{\hat{\mathbf{e}}}}. \tag{14}$$

Fig. 6 depicts the calculated L_s based on the FEA results, $L_{s,\mathrm{FEA}}$ with respect to $\mathbf{i}_{\mathbf{dqs}}^{\hat{\mathbf{e}}}$ in (12) and (13). In Fig. 6, $L_{s,\mathrm{FEA}}$ is saturated not only by d-axis current, but also by the q-axis current due to cross-saturation. Although the FEA can reflect the magnetic characteristics of IM qualitatively, there would

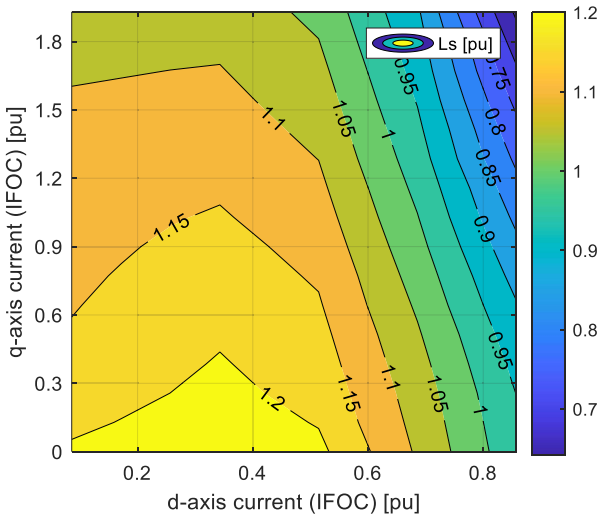

Fig. 6. FEA-based stator inductance map.

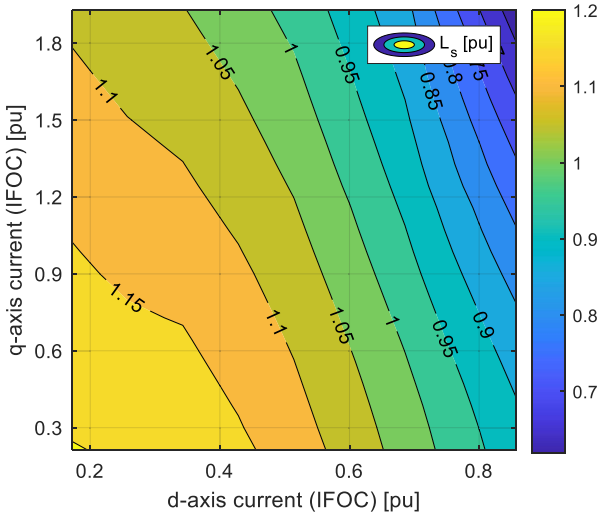

Fig. 7. FEA-based stator inductance map modified with experimental results.

be a discrepancy with the actual experimental tests. For example, $L_{s,\mathrm{FEA}}(i^{\hat{e}}_{ds}, 0)$ at no-load condition does not match to $L_{s,\mathrm{EXP}}(I_{s0})$ in Fig. 4. Therefore, using the FEA results in Fig. 6 directly to the experimental parameter commissioning would result in a considerable error, and it should be modified to reduce the discrepancy with the experimental results. In this article, $L_{s,\mathrm{MOD}}$ is defined as follows:

$$L_{s,\mathrm{MOD}}(i^{\hat{e}}_{ds}, i^{\hat{e}}_{qs}) = L_{s,\mathrm{FEA}}(i^{\hat{e}}_{ds}, i^{\hat{e}}_{qs}) \cdot \frac{L_{s,\mathrm{EXP}}(i^{\hat{e}}_{ds})}{L_{s,\mathrm{FEA}}(i^{\hat{e}}_{ds}, 0)}. \quad (15)$$

$L_{s,\mathrm{MOD}}\ (i^{\hat{e}}_{ds}, i^{\hat{e}}_{qs})$ denotes the modified L_s at $(i^{\hat{e}}_{ds}, i^{\hat{e}}_{qs})$. Fig. 7 shows the $L_{s,\mathrm{MOD}}$ with respect to $\mathbf{i}^{\hat{e}}_{\mathbf{dqs}}$. It should be noted that $\mathbf{i}^{\hat{e}}_{\mathbf{dqs}}$ is not the actual dq-axis current at rotor flux reference frame, but the calculated current vector under IFOC with a constant τ_{r0}.

The modified map not only has the cross-saturation characteristics of FEA results, but also well corresponds with the experimental results in Fig. 4. The map of $L_{s,\mathrm{MOD}}$ in Fig. 7 can be utilized as a preset L_s map to solve the rank deficiency problem.

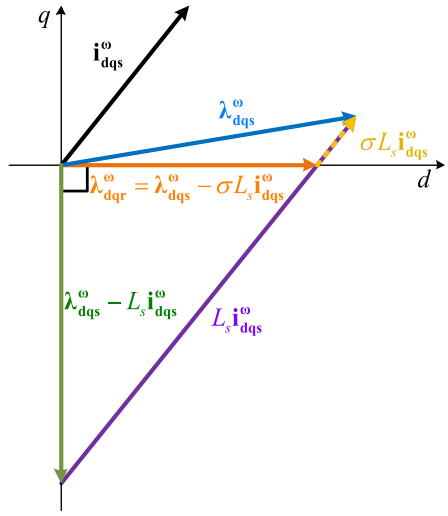

Fig. 8. Orthogonality between $\boldsymbol{\lambda}^{\omega}_{\mathbf{dqr}}$ and $\boldsymbol{\lambda}^{\omega}_{\mathbf{dqs}} - L_s \mathbf{i}^{\omega}_{\mathbf{dqs}}$.

Through the preset L_s map in Fig. 7, the other parameters, e.g., σL_s and R_r, can be experimentally calculated.

D. σL_s and R_r Calculation

The leakage inductance and the rotor resistance, i.e., σL_s and R_r, can be obtained based on the preset L_s map and (8). Equation (8) can be rewritten as follows by multiplying ${\boldsymbol{\lambda}^{\omega}_{\mathbf{dqr}}}^{\mathbf{T}}$:

$$R_r {\boldsymbol{\lambda}^{\omega}_{\mathbf{dqr}}}^{\mathbf{T}} \mathbf{i}^{\omega}_{\mathbf{dqs}} = {\boldsymbol{\lambda}^{\omega}_{\mathbf{dqr}}}^{\mathbf{T}} \left(\frac{R_r}{L_m} + \omega_{sl} \mathbf{J} \right) \boldsymbol{\lambda}^{\omega}_{\mathbf{dqr}}. \quad (16)$$

The superscript "$\mathbf{T}$" denotes the transpose operator. Since $\mathbf{x}^{\mathbf{T}}\mathbf{J}\mathbf{x} = 0$ for an arbitrary vector $\mathbf{x}$, (16) can be simplified as

$$L_m {\boldsymbol{\lambda}^{\omega}_{\mathbf{dqr}}}^{\mathbf{T}} \mathbf{i}^{\omega}_{\mathbf{dqs}} = {\boldsymbol{\lambda}^{\omega}_{\mathbf{dqr}}}^{\mathbf{T}} \boldsymbol{\lambda}^{\omega}_{\mathbf{dqr}}. \quad (17)$$

From (6) and (17), the following equation can be derived:

$$\left(\boldsymbol{\lambda}^{\omega}_{\mathbf{dqs}} - \sigma L_s \mathbf{i}^{\omega}_{\mathbf{dqs}} \right)^{\mathbf{T}} \left(\boldsymbol{\lambda}^{\omega}_{\mathbf{dqs}} - L_s \mathbf{i}^{\omega}_{\mathbf{dqs}} \right) = 0. \quad (18)$$

Thus, σL_s at an arbitrary operating point can be calculated as

$$\sigma L_s = \frac{||\boldsymbol{\lambda}^{\omega}_{\mathbf{dqs}}||^2 - L_s {\boldsymbol{\lambda}^{\omega}_{\mathbf{dqs}}}^{\mathbf{T}} \mathbf{i}^{\omega}_{\mathbf{dqs}}}{{\mathbf{i}^{\omega}_{\mathbf{dqs}}}^{\mathbf{T}} \boldsymbol{\lambda}^{\omega}_{\mathbf{dqs}} - L_s ||\mathbf{i}^{\omega}_{\mathbf{dqs}}||^2}. \quad (19)$$

Equation (18) can be interpreted by the vector diagram in Fig. 8. It can be noted that $\boldsymbol{\lambda}^{\omega}_{\mathbf{dqr}}$ is always perpendicular to $\boldsymbol{\lambda}^{\omega}_{\mathbf{dqs}} - L_s \mathbf{i}^{\omega}_{\mathbf{dqs}}$ regardless of the parameter variation.

The rotor resistance can be similarly calculated from (8). Equation (8) can be rewritten as follows by multiplying ${\boldsymbol{\lambda}^{\omega}_{\mathbf{dqr}}}^{\mathbf{T}}\mathbf{J}$:

$$R_r {\boldsymbol{\lambda}^{\omega}_{\mathbf{dqr}}}^{\mathbf{T}} \mathbf{J} \mathbf{i}^{\omega}_{\mathbf{dqs}} = -\omega_{sl} {\boldsymbol{\lambda}^{\omega}_{\mathbf{dqr}}}^{\mathbf{T}} \boldsymbol{\lambda}^{\omega}_{\mathbf{dqr}}. \quad (20)$$

Therefore, R_r at an arbitrary operating point can be calculated as

$$R_r = -\omega_{sl} \frac{||\boldsymbol{\lambda}^{\omega}_{\mathbf{dqs}} - \sigma L_s \mathbf{i}^{\omega}_{\mathbf{dqs}}||^2}{{\boldsymbol{\lambda}^{\omega}_{\mathbf{dqs}}}^{\mathbf{T}} \mathbf{J} \mathbf{i}^{\omega}_{\mathbf{dqs}}}. \quad (21)$$

It should be noted that (19) and (21) are valid regardless of the reference frame. Therefore, using (19) and (21), σL_s and R_r can

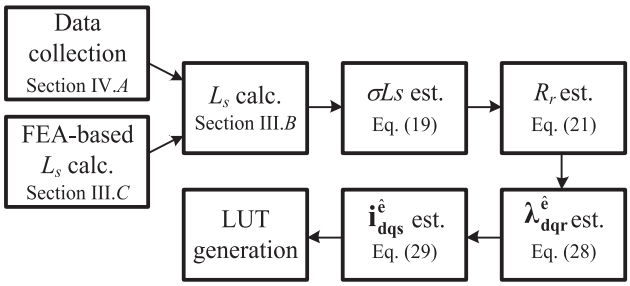

Fig. 9. Proposed procedure for IM parameter LUT generation.

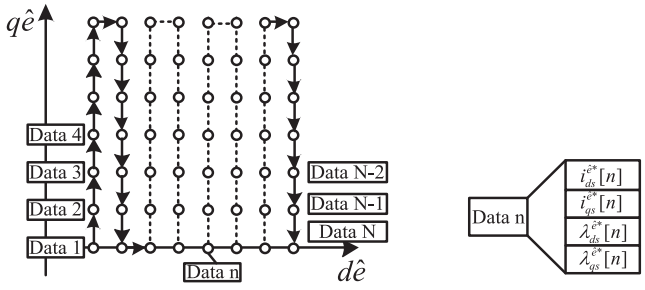

(a) (b)

Fig. 10. (a) Data collection procedure. (b) Collected information.

be calculated even if the reference frame is not synchronized to the actual rotor flux, e.g., IFOC with preset rotor time constant. Besides σL_s and R_r, the mutual inductance L_m can be easily calculated as $L_m = L_s - \sigma L_s$ from (9).

IV. Implementation of Proposed Method

As discussed in the Section III, for a certain operating point, the motor parameters, i.e., L_s, σL_s, R_r, and L_m, can be estimated for a certain operating point even when the rotor flux position is unknown. However, the obtained information is not directly applicable as a parameter LUT for FOC because the measured operating points are not uniformly arranged in the dq-axis plane with accurate rotor flux orientation. In this section, the implementation procedure to convert the obtained parameter set into a parameter LUT for FOC is discussed, as shown in Fig. 9. This section primarily focuses on the data collection procedure and the postprocessing of the obtained data, in addition to the parameter estimation methods.

A. Data Collection Procedure

To construct the experimental parameter map with the process in Section III, the stator flux information should be collected at each operating point. Fig. 10(a) and (b) shows the data collection procedure and the collected information at each operating point. The total number of the data points is denoted as N. During the procedure, the load machine regulates the shaft speed at a fixed speed ω_{r0}, and the stator current and stator flux information of the target motor are obtained by changing the current magnitude and the slip frequency ω_{sl}. Unlike the FEA process, it is not easy to obtain the accurate rotor flux reference frame in the experiment, so the target IM is controlled under IFOC with the

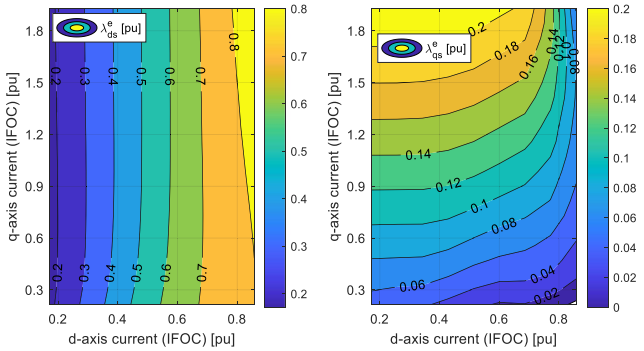

(a) (b)

Fig. 11. Collected stator flux information. (a) $\lambda^{\hat{e}}_{ds}(i^{\hat{e}}_{ds}, i^{\hat{e}}_{qs})$. (b) $\lambda^{\hat{e}}_{qs}(i^{\hat{e}}_{ds}, i^{\hat{e}}_{qs})$.

rotor time constant τ_{r0}. At the nth data, the synchronous speed $\omega_e[n]$ is calculated as

$$\omega_e[n] = \omega_{r0} + \omega_{sl}[n] \tag{22}$$

where

$$\omega_{sl}[n] = \frac{1}{\tau_{r0}} \frac{i^{\hat{e}}_{qs}[n]}{i^{\hat{e}}_{ds}[n]}. \tag{23}$$

The synchronous reference angle is calculated by integrating $\omega_e[n]$. At each point, the stator flux can be calculated as

$$\boldsymbol{\lambda}^{\hat{\mathbf{e}}}_{\mathbf{dqs}}[n] = -\mathbf{J} \frac{\mathbf{v}^{\hat{\mathbf{e}}}_{\mathbf{dqs}}[n] - R_s \mathbf{i}^{\hat{\mathbf{e}}}_{\mathbf{dqs}}[n]}{\omega_e[n]}. \tag{24}$$

Fig. 11(a) and (b) depicts the experimentally collected stator flux information. Although the data are collected by changing the current magnitude and the slip frequency, Fig. 11(a) and (b) is plotted with respect to the dq-axis current vector under IFOC for better readability. As in the L_s estimation, the shaft speed is regulated as half of the base speed during the data acquisition. During the data acquisition, the rotor temperature may increase due to the current flow in the rotor bar, and R_r would vary during the experiments. Therefore, the rotor temperature should be kept in a certain range by providing a sufficient time interval during the tests.

B. LUT Construction

As aforementioned, since $\boldsymbol{\lambda}^{\hat{\mathbf{e}}}_{\mathbf{dqs}}(i^{\hat{e}}_{ds}, i^{\hat{e}}_{qs})$ in Fig. 11 and $L_{s,\mathrm{MOD}}(i^{\hat{e}}_{ds}, i^{\hat{e}}_{qs})$ in Fig. 7 are built based on the IFOC with τ_{r0}, the motor parameters at nth data can be calculated as follows using (19) and (21):

$$\hat{\sigma}\hat{L}_s[n] = \frac{||\boldsymbol{\lambda}^{\hat{\mathbf{e}}}_{\mathbf{dqs}}[n]||^2 - \hat{L}_s[n] \cdot \left(\boldsymbol{\lambda}^{\hat{\mathbf{e}}}_{\mathbf{dqs}}[n]^{\mathbf{T}} \mathbf{i}^{\hat{\mathbf{e}}}_{\mathbf{dqs}}[n]\right)}{\left(\mathbf{i}^{\hat{\mathbf{e}}}_{\mathbf{dqs}}[n]^{\mathbf{T}} \boldsymbol{\lambda}^{\hat{\mathbf{e}}}_{\mathbf{dqs}}[n]\right) - \hat{L}_s[n] \cdot ||\mathbf{i}^{\hat{\mathbf{e}}}_{\mathbf{dqs}}[n]||^2} \tag{25}$$

$$\hat{R}_r[n] = -\omega_{sl}[n] \frac{||\boldsymbol{\lambda}^{\hat{\mathbf{e}}}_{\mathbf{dqs}}[n] - \hat{\sigma}\hat{L}_s[n] \cdot \mathbf{i}^{\hat{\mathbf{e}}}_{\mathbf{dqs}}[n]||^2}{\boldsymbol{\lambda}^{\hat{\mathbf{e}}}_{\mathbf{dqs}}[n]^{\mathbf{T}} \mathbf{J} \mathbf{i}^{\hat{\mathbf{e}}}_{\mathbf{dqs}}[n]} \tag{26}$$

where

$$\hat{L}_s[n] = L_{s,\mathrm{MOD}}(i^{\hat{e}}_{ds}[n], i^{\hat{e}}_{qs}[n]). \tag{27}$$

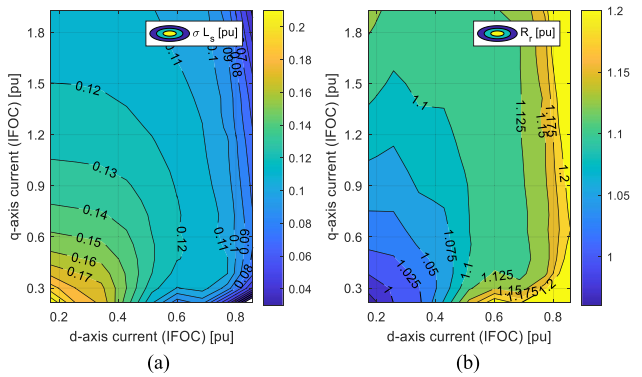

Fig. 12. Calculated motor parameters. (a) $\sigma L_s(i^{\hat{e}}_{ds}, i^{\hat{e}}_{qs})$. (b) $R_r(i^{\hat{e}}_{ds}, i^{\hat{e}}_{qs})$.

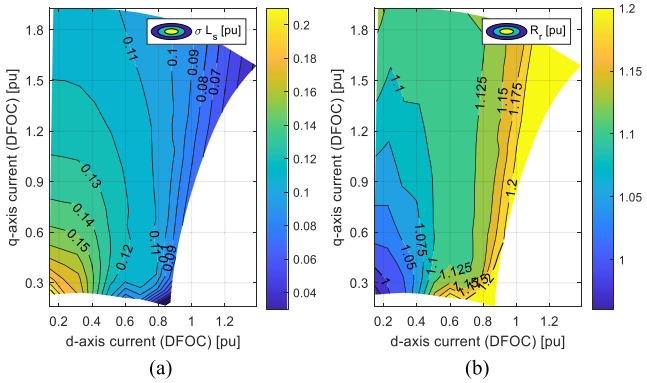

Fig. 13. Motor parameters in terms of $\mathbf{i^e_{dqs}}$. (a) $\sigma L_s(i^e_{ds}, i^e_{qs})$. (b) $R_r(i^e_{ds}, i^e_{qs})$.

The calculated σL_s and R_r are shown in Fig. 12(a) and (b). It can be noticed that both σL_s and R_r are varying according to the operating point. Especially, σL_s is saturated as the current magnitude increases, and it is well-matched with the physical sense. However, Fig. 12(a) and (b) cannot be used as the parameter LUT for the online flux estimation. The reference domain, where the data are collected, is the current vector in IFOC, not the DFOC with accurate parameters. Therefore, the axis would not be aligned to the actual rotor flux.

To solve the problem, this article proposes the recalculation of the actual rotor flux reference frame at each data point. For the nth data, the rotor flux can be calculated as

$$\boldsymbol{\lambda}^{\hat{\mathbf{e}}}_{\mathbf{dqr}}[n] = \boldsymbol{\lambda}^{\hat{\mathbf{e}}}_{\mathbf{dqs}}[n] - \sigma L_s[n] \cdot \mathbf{i}^{\hat{\mathbf{e}}}_{\mathbf{dqs}}[n]. \tag{28}$$

From (28), the current vector at the rotor flux reference frame can be calculated as

$$\mathbf{i}^{\mathbf{e}}_{\mathbf{dqs}} = \mathbf{R}(-\text{atan2}(\lambda^{\hat{e}}_{qr}, \lambda^{\hat{e}}_{dr})) \cdot \mathbf{i}^{\hat{\mathbf{e}}}_{\mathbf{dqs}} \tag{29}$$

where $\mathbf{R}(\theta)$ is the rotational operator with angle θ. The superscript "e" denotes the rotor flux reference frame. The motor parameters can be represented with respect to $\mathbf{i}^{\mathbf{e}}_{\mathbf{dqs}}$, as shown in Fig. 13(a) and (b). Due to the discrepancy between $\mathbf{i}^{\hat{\mathbf{e}}}_{\mathbf{dqs}}$ and $\mathbf{i}^{\mathbf{e}}_{\mathbf{dqs}}$, the test region is highly distorted in the perspective of $\mathbf{i}^{\mathbf{e}}_{\mathbf{dqs}}$.

Fig. 14(a)–(d) shows the motor parameter LUTs, constructed by interpolating Fig. 13(a) and (b) with a uniformly spaced plane. The "griddata" function of MATLAB software has been adopted for the 2-D interpolation. The parameter LUTs in Fig. 14(a)–(d) can be utilized in the actual operation of IM, and accurate rotor flux-oriented control (RFOC) can be achieved.

C. Flux Estimation Based on Proposed Parameter LUTs

It can be observed that L_s, L_m, and σL_s in (9) are the static inductances, not the incremental inductances which are derivative of the flux with respect to the current. Therefore, it is important to select a proper flux observer which is constructed based on the static inductance parameters. Among various flux observer, the flux observers in [17], which takes the stator flux and rotor flux as the state variables, can take advantages of the proposed parameter LUTs.

In [17], the stator and rotor flux vectors can be estimated as

$$\begin{aligned}\frac{d}{dt}\begin{bmatrix}\hat{\boldsymbol{\lambda}}^{\mathbf{e}}_{\mathbf{dqs}}\\ \hat{\boldsymbol{\lambda}}^{\mathbf{e}}_{\mathbf{dqr}}\end{bmatrix} &= \begin{bmatrix}-\frac{1}{\hat{\sigma}\hat{L}_s}\hat{R}_s - \omega_e\mathbf{J} & -\frac{1}{\hat{\sigma}\hat{L}_s}R_s\\ \hat{R}_r & -\left(\hat{R}_r/\hat{L}_m + \omega_{sl}\mathbf{J}\right)\end{bmatrix}\\ &\quad\times\begin{bmatrix}\hat{\boldsymbol{\lambda}}^{\mathbf{e}}_{\mathbf{dqs}}\\ \hat{\boldsymbol{\lambda}}^{\mathbf{e}}_{\mathbf{dqr}}\end{bmatrix}\\ &\quad+\begin{bmatrix}\mathbf{I}\\ 0\end{bmatrix}\mathbf{v}^{\mathbf{e}}_{\mathbf{dqs}} + \mathbf{K}\left(\mathbf{i}^{\mathbf{e}}_{\mathbf{dqs}} - \hat{\mathbf{i}}^{\mathbf{e}}_{\mathbf{dqs}}\right)\end{aligned} \tag{30}$$

where

$$\hat{\mathbf{i}}^{\mathbf{e}}_{\mathbf{dqs}} = \frac{1}{\hat{\sigma}\hat{L}_s}\left(\hat{\boldsymbol{\lambda}}^{\mathbf{e}}_{\mathbf{dqs}} - \hat{\boldsymbol{\lambda}}^{\mathbf{e}}_{\mathbf{dqr}}\right). \tag{31}$$

The estimated stator flux and the rotor flux at the synchronous reference frame are represented by $\hat{\boldsymbol{\lambda}}^{\mathbf{e}}_{\mathbf{dqs}}$ and $\hat{\boldsymbol{\lambda}}^{\mathbf{e}}_{\mathbf{dqr}}$. Concerning the gain matrix $\mathbf{K}$, the observer in (30) is inherently stable even with a null $\mathbf{K}$. Of course, it can be adjusted through various gain scheduling methods to achieve additional robustness against parameter mismatch. Nevertheless, as the primary purpose of this article is to present a process to obtain an accurate parameter set, the experimental verification in the next section using the flux observer is conducted with null $\mathbf{K}$.

An exemplary control block diagram of DFOC with the proposed parameter LUTs is demonstrated in Fig. 15. The superscripts "$*$" and "$\hat{}$" denote the reference value and the estimated value, respectively. For example, $T_e{}^*$ denotes the torque reference value. The rotor flux angle θ_e can be estimated by nullifying $\hat{\lambda}^e_{qr}$ through a phase-locked loop. The parameters in (30) are updated based on the proposed LUTs at every sampling time. Moreover, the current regulator gain can be adjusted accordingly. It should be noted that Fig. 15 is a basic block diagram for RFOC. It is expected that the advanced controllers, such as flux regulator or overmodulation schemes, can be implemented without losing the advantages of the proposed parameter LUTs.

V. Experimental Verification

The feasibility of the obtained parameter LUTs is verified with the experimental tests. The experimental setup in Fig. 3(a) and (b) has been used in the experimental verification. During the experiments, the dc-link voltage is set as 330 V, and the

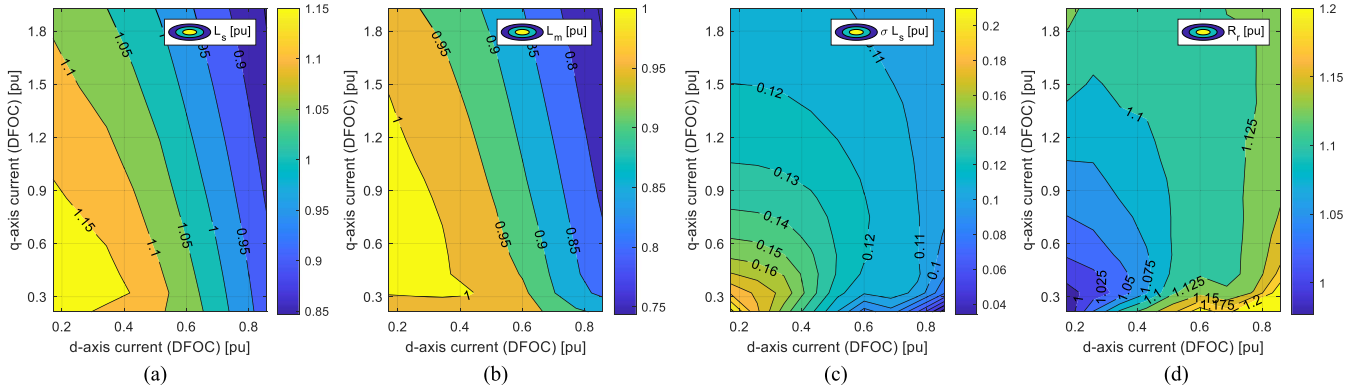

Fig. 14. Interpolated motor parameter LUTs. (a) $L_s(i^e_{ds}, i^e_{qs})$. (b) $L_m(i^e_{ds}, i^e_{qs})$. (c) $\sigma L_s(i^e_{ds}, i^e_{qs})$. (d) $R_r(i^e_{ds}, i^e_{qs})$.

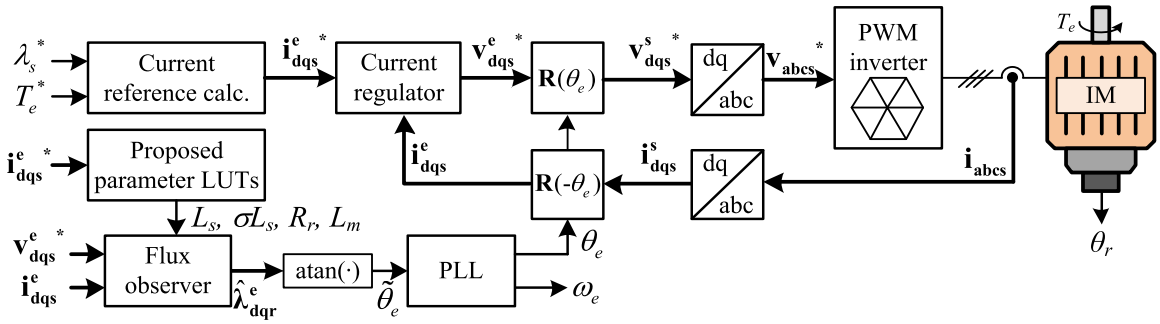

Fig. 15. Control block diagram with proposed parameter LUTs.

inverter operates at 10 kHz of the switching frequency. The TI-TMS320F28377D has been selected for the microprocessor of the inverter. While the microprocessor has two distinct computation cores, but only one core has been dedicated for driving both the motor and load machine in the experimental verification. The LUTs in Fig. 14(a)–(d) have been selected for the parameter LUTs under tests. As aforementioned, the parameter LUTs are obtained at $\omega_r = 0.5$ per unit (p.u.).

Prior to evaluating the performance of DFOC with the proposed parameter LUTs, the accuracy of the parameter LUTs itself should be validated. Unfortunately, directly verifying the accuracy of the obtained parameter LUT experimentally is challenging. To address this issue, this article compares the stator voltage with an estimated stator voltage calculated by the proposed parameter LUTs, as shown in Fig. 16. In Fig. 16, the ω_{rm} is the rotor speed in the mechanical angle, and the current controller is abbreviated as "CC." The target motor is run by two algorithms; one is the IFOC with the nominal parameters, and the other is the IFOC with the proposed parameter LUTs. For the IFOC with the nominal parameters, nominal parameters $R_{r,\text{nominal}}$ and $L_{m,\text{nominal}}$ are set as 1.0 and 0.83 p.u., respectively. In the latter case, the slip frequency is set as follows:

$$\omega^*_{sl} = \frac{\hat{R}_r(i^{\hat{e}}_{ds}{}^*, i^{\hat{e}}_{qs}{}^*)}{\hat{L}_m(i^{\hat{e}}_{ds}{}^*, i^{\hat{e}}_{qs}{}^*)} \frac{i^{\hat{e}}_{qs}{}^*}{i^{\hat{e}}_{ds}{}^*}. \tag{32}$$

$i^{\hat{e}}_{ds}$ and $i^{\hat{e}}_{qs}$ are the dq-axes current references, and $\omega_{sl}{}^*$ is the commanded slip frequency. The stator voltage can be estimated

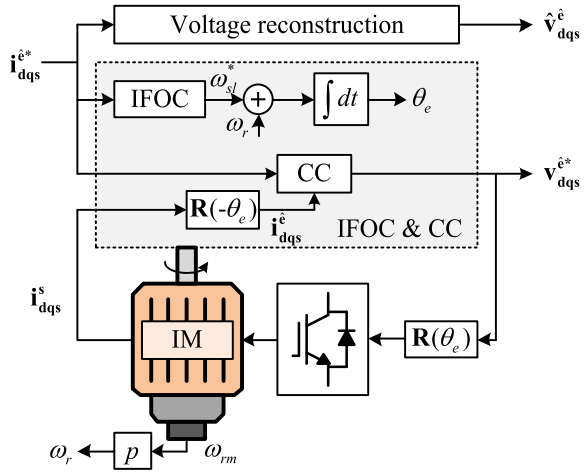

Fig. 16. Voltage reconstruction.

by adding the leakage flux to the rotor flux as follows.

$$\hat{\mathbf{v}}^{\hat{\mathbf{e}}}_{\mathbf{dqs}} = R_s \mathbf{i}^{\hat{\mathbf{e}}*}_{\mathbf{dqs}} + \omega_e \mathbf{J} \hat{\boldsymbol{\lambda}}^{\hat{\mathbf{e}}}_{\mathbf{dqs}} \tag{33}$$

where

$$\hat{\boldsymbol{\lambda}}^{\hat{\mathbf{e}}}_{\mathbf{dqs}} = \frac{\hat{L}_m(i^{\hat{e}}_{ds}{}^*, i^{\hat{e}}_{qs}{}^*) \cdot \hat{R}_r(i^{\hat{e}}_{ds}{}^*, i^{\hat{e}}_{qs}{}^*)}{\hat{L}_m(i^{\hat{e}}_{ds}{}^*, i^{\hat{e}}_{qs}{}^*)s + \hat{R}_r(i^{\hat{e}}_{ds}{}^*, i^{\hat{e}}_{qs}{}^*)} \mathbf{i}^{\hat{\mathbf{e}}*}_{\mathbf{dqs}} + \hat{\sigma}\hat{L}_s(i^{\hat{e}}_{ds}{}^*, i^{\hat{e}}_{qs}{}^*) \mathbf{i}^{\hat{\mathbf{e}}*}_{\mathbf{dqs}}. \tag{34}$$

The accuracy of the parameter LUTs can be evaluated indirectly by comparing the estimated voltage in (33) to the

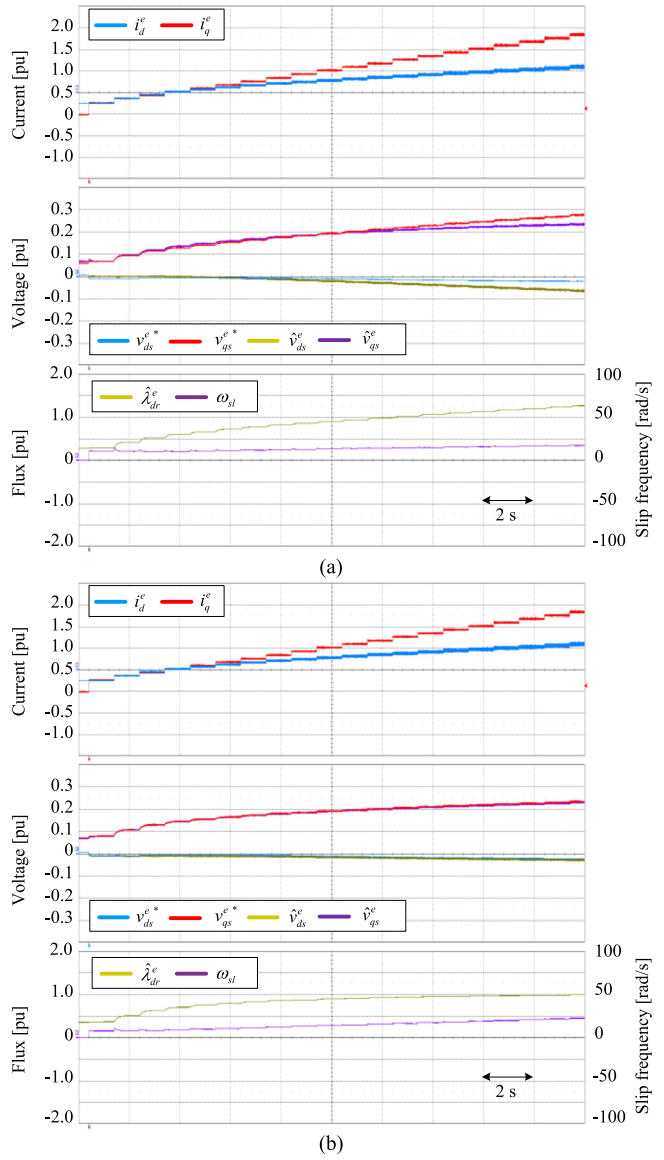

Fig. 17. Experimental results. (a) IFOC with nominal parameters. (b) IFOC with proposed parameter LUTs.

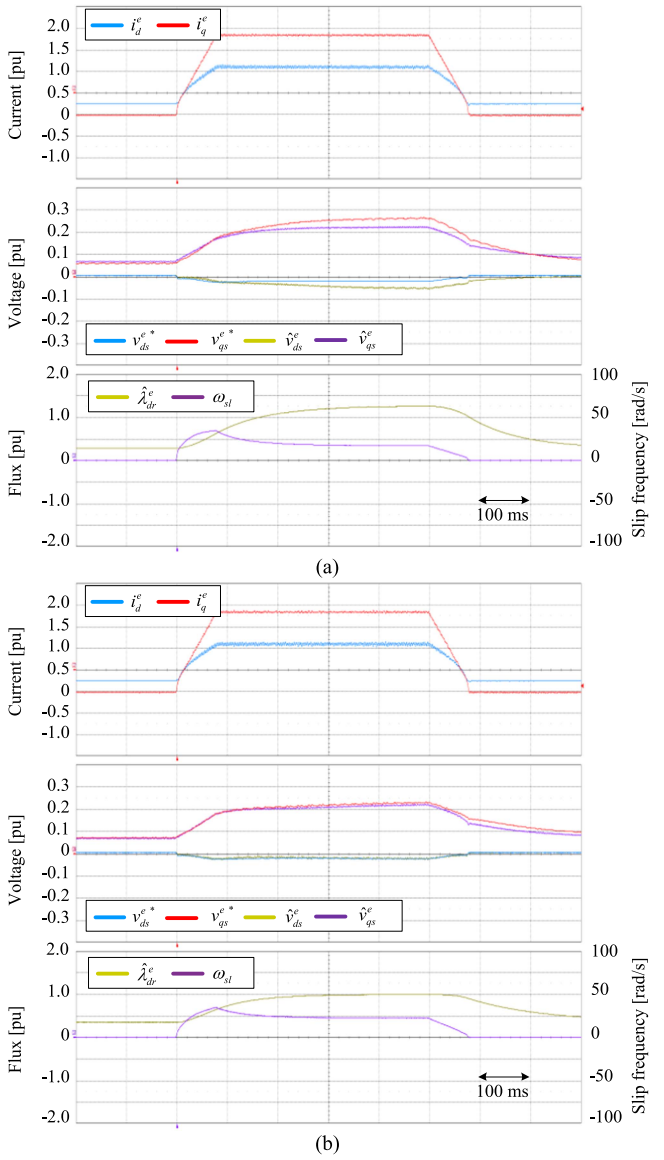

Fig. 18. Experimental results at transient situation. (a) IFOC with nominal parameters. (b) IFOC with proposed parameter LUTs.

actual voltage vector $\mathbf{v}_{\mathbf{dqs}}^{\hat{\mathbf{e}}\,*}$, which is the output of the current controller. Fig. 17(a) and (b) depicts the experimental results changing the torque reference from zero to the maximum torque rating. The current reference is set along the maximum torque-per-Ampere trajectory. The rotor speed is set as 0.25 p.u. for both cases. In Fig. 17(a), the IFOC with the nominal parameters has an error between the actual voltage reference and the estimated voltage vector in (33), which would come from the flux estimation error. In contrast, as shown in Fig. 17(b), the voltage estimation error is conspicuously reduced in the IFOC with the proposed parameter LUTs.

Fig. 18(a) and (b) shows the experimental waveforms observed during a transient load test. The current reference of maximum torque is applied to the target motor with a slew rate of 20 p.u./s. As in Fig. 17, the rotor speed is set as 0.25 p.u. Due to the rapid change in *d*-axis current, the rotor flux experiences nonlinear changes according to the nonlinear rotor time constant, which would be reflected in the stator voltage. In Fig. 18(a), it is observed that the actual stator voltage deviates significantly from the estimated stator voltage in the IFOC with the nominal rotor time constant. This discrepancy indicates that the nominal rotor time constant is insufficient to estimate the angle of the rotor flux accurately during the transient. Conversely, in Fig. 18(b), it can be observed that the proposed parameter LUTs can accurately estimate the stator voltage even in the transient situation. These results demonstrate that the proposed LUTs provide a more accurate value of the rotor time constant, enabling accurate FOC of IM in a dynamic situation.

The proposed parameter LUTs are not only beneficial for IFOC, but they can also enhance the performance of a rotor flux observer for DFOC. To assess the torque accuracy of the DFOC with the proposed LUTs, the torque reference changes

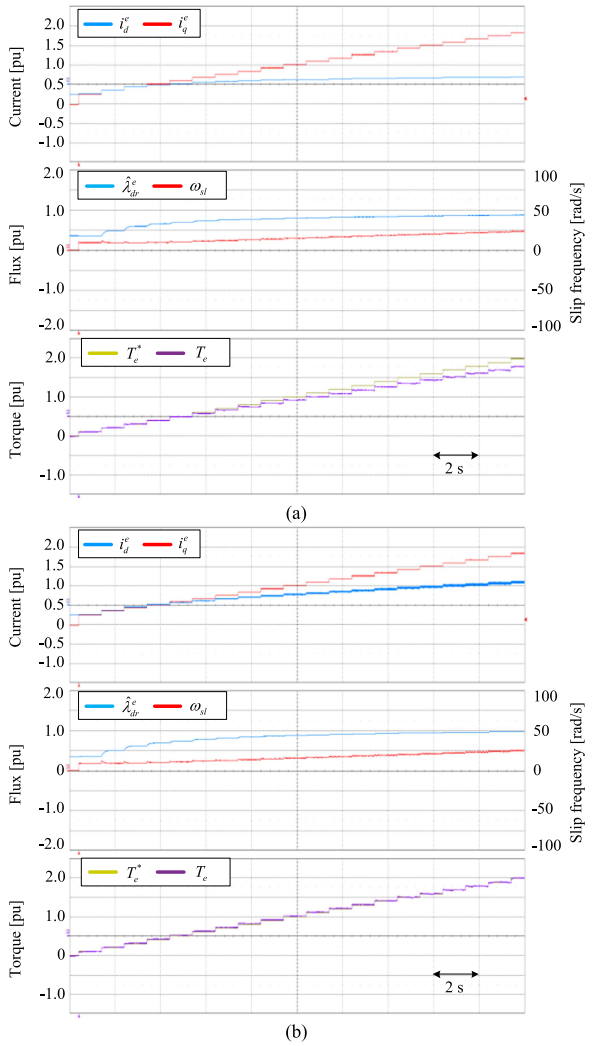

Fig. 19. Experimental results of DFOC (a) with nominal parameters and (b) with proposed parameter LUTs.

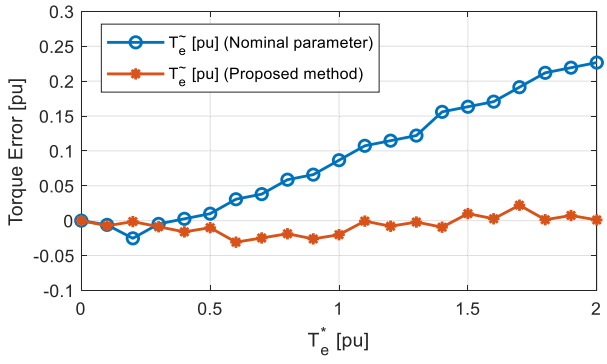

Fig. 20. Comparison of torque error.

from null to the maximum torque in Fig. 19. During the test, the speed is regulated at 1 p.u., the base speed. Fig. 19(a) depicts the experimental results of DFOC with nominal parameters. It can be noticed that the torque error magnifies as the torque reference increases. It would stem from the parameter variation in high-torque operating condition. On the other hand, it can be

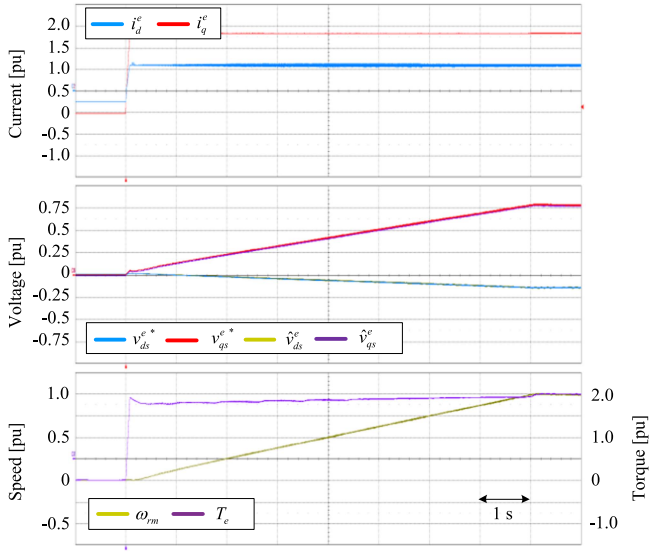

Fig. 21. Experimental results of DFOC with proposed parameter LUTs under speed acceleration.

noticed that the DFOC with the proposed parameter LUTs provides accurate torque control performance in the whole torque range, as shown in Fig. 19(b).

Fig. 20 quantitatively compares the torque errors in both cases, i.e., $T_e{}^*$–T_e. When the nominal parameter set is applied, the torque error increases up to 22% of the rated torque. Notably, the proposed method keeps the maximum torque error within only 3% of the rated torque. This result demonstrates the feasibility of the proposed parameter LUTs in accurate torque control of IM drive.

The performance of the DFOC with the proposed LUTs under the speed variation is demonstrated in Fig. 21. The target motor applies the maximum torque that is twice the continuous rated torque, while the load machine increases the shaft speed from zero to the base speed. The test results establish that the proposed LUTs are effective throughout the entire speed range.

VI. Conclusion

This article presents a procedure for identifying the parameters of IMs. Unlike the previous methods, the proposed procedure does not limit the identification range to a specific operating point or nominal parameters. Instead, the proposed method can provide a set of parameter LUTs for the entire region of dq-axis current. In the identification procedure, all inductance variables and rotor resistance are assumed to vary with the operating point. To address the rank deficiency problem between the IM model equations and the unknown parameters, the stator inductance is preset based on FEA. The proposed parameter identification is verified with the experimental tests. It is demonstrated that the proposed method can estimate the accurate motor parameters by comparing the actual voltage and the reconstructed voltage vector based on the proposed LUTs. In addition, it is shown that the proposed parameter LUTs are also effective in enhancing the control performance of flux estimation for DFOC.

REFERENCES

[1] S. Bozhko, S. Dymko, S. Kovbasa, and S. M. Peresada, "Maximum torque-per-amp control for traction IM drives: Theory and experimental results," *IEEE Trans. Ind. Appl.*, vol. 53, no. 1, pp. 181–193, Jan./Feb. 2017, doi: 10.1109/TIA.2016.2608789.

[2] M. Stender, O. Wallscheid, and J. Böcker, "Accurate torque control for induction motors by utilizing a globally optimized flux observer," *IEEE Trans. Power Electron.*, vol. 36, no. 11, pp. 13261–13274, Nov. 2021, doi: 10.1109/TPEL.2021.3080129.

[3] S. A. Odhano, P. Pescetto, H. A. A. Awan, M. Hinkkanen, G. Pellegrino, and R. Bojoi, "Parameter identification and self-commissioning in AC motor drives: A technology status review," *IEEE Trans. Power Electron.*, vol. 34, no. 4, pp. 3603–3614, Apr. 2019, doi: 10.1109/TPEL.2018.2856589.

[4] S.-H. Lee, A. Yoo, H.-J. Lee, Y.-D. Yoon, and B.-M. Han, "Identification of induction motor parameters at standstill based on integral calculation," *IEEE Trans. Ind. Appl.*, vol. 53, no. 3, pp. 2130–2139, May/Jun. 2017, doi: 10.1109/TIA.2017.2650141.

[5] L. Monjo, H. Kojooyan-Jafari, F. Córcoles, and J. Pedra, "Squirrel-cage induction motor parameter estimation using a variable frequency test," *IEEE Trans. Energy Convers.*, vol. 30, no. 2, pp. 550–557, Jun. 2015, doi: 10.1109/TEC.2014.2362964.

[6] D. M. Reed, H. F. Hofmann, and J. Sun, "Offline identification of induction machine parameters with core loss estimation using the stator current locus," *IEEE Trans. Energy Convers.*, vol. 31, no. 4, pp. 1549–1558, Dec. 2016, doi: 10.1109/TEC.2016.2601781.

[7] X. Chen, J. Wang, B. Sen, P. Lazari, and T. Sun, "A high-fidelity and computationally efficient model for interior permanent-magnet machines considering the magnetic saturation, spatial harmonics, and iron loss effect," *IEEE Trans. Ind. Electron.*, vol. 62, no. 7, pp. 4044–4055, Jul. 2015, doi: 10.1109/TIE.2014.2388200.

[8] D. Hu, Y. M. Alsmadi, and L. Xu, "High-fidelity nonlinear IPM modeling based on measured stator winding flux linkage," *IEEE Trans. Ind. Appl.*, vol. 51, no. 4, pp. 3012–3019, Jul./Aug. 2015, doi: 10.1109/TIA.2015.2407864.

[9] J. Lee, Y.-C. Kwon, and S.-K. Sul, "Identification of IPMSM flux-linkage map for high-accuracy simulation of IPMSM drives," *IEEE Trans. Power Electron.*, vol. 36, no. 12, pp. 14257–14266, Dec. 2021, doi: 10.1109/TPEL.2021.3084558.

[10] J.-H. Lee, Y.-C. Kwon, and S.-K. Sul, "High-fidelity induction motor simulation model based on finite element analysis," *IEEE Trans. Ind. Electron.*, vol. 69, no. 10, pp. 9872–9883, Oct. 2022, doi: 10.1109/TIE.2022.3163556.

[11] D. Lin, P. Zhou, and Z. Zhang, "Reduced order modeling and parameter identification of induction motors based on FEA solutions," *IEEE Trans. Energy Convers.*, vol. 38, no. 2, pp. 1108–1117, Jun. 2023, doi: 10.1109/TEC.2022.3227417.

[12] J. Kullick and C. M. Hackl, "Nonlinear modeling, identification, and optimal feedforward torque control of induction machines using steady-state machine maps," *IEEE Trans. Ind. Electron.*, vol. 70, no. 1, pp. 211–221, Jan. 2023, doi: 10.1109/TIE.2022.3153811.

[13] J. Yoo, J.-H. Lee, and S.-K. Sul, "FEA-assisted experimental parameter identification of induction motor," in *Proc. IEEE Int. Power Electron. Conf.*, 2022, pp. 789–794, doi: 10.23919/IPEC-Himeji2022-ECCE53331.2022.9807077.

[14] Y. Park and S.-K. Sul, "A novel method utilizing trapezoidal voltage to compensate for inverter nonlinearity," *IEEE Trans. Power Electron.*, vol. 27, no. 12, pp. 4837–4846, Dec. 2012, doi: 10.1109/TPEL.2012.2192451.

[15] N. Bedetti, S. Calligaro, and R. Petrella, "Self-commissioning of inverter dead-time compensation by multiple linear regression based on a physical model," *IEEE Trans. Ind. Appl.*, vol. 51, no. 5, pp. 3954–3964, Sep./Oct. 2015, doi: 10.1109/TIA.2015.2436882.

[16] S.-K. Sul, *Control of Electric Machine Drive Systems*. Hoboken, NJ, USA: Wiley, 2010.

[17] M. Hinkkanen and J. Luomi, "Parameter sensitivity of full-order flux observers for induction motors," *IEEE Trans. Ind. Appl.*, vol. 39, no. 4, pp. 1127–1135, Jul./Aug. 2003, doi: 10.1109/TIA.2003.814560.

Jiwon Yoo (Member, IEEE) received the B.S. and Ph.D. degrees in electrical and computer engineering from Seoul National University, Seoul, South Korea, in 2017 and 2022, respectively.

From 2014 to 2017, he was a Research Engineer with Seoho Electric Company, Anyang, South Korea. From 2022 to 2023, he was a Senior Research Engineer with the Hyundai Motor Company, Seongnam, South Korea. Since 2023, he has been with Inha University, Incheon, South Korea, where he is currently an Assistant Professor. His current research interests include power electronics, control of electric machines, power semiconductors, and sensorless drives.

Dr. Yoo was the recipient of the Best Paper Award First Prize at 2019 International Conference on Power Electronics (ICPE-Busan/ECCE-Asia) and the Best Paper Award at 2020 International Power Electronics and Motion Control Conference (IPEMC-Nanjing/ECCE-Asia).

Joon-Hee Lee (Member, IEEE) was born in South Korea in 1990. He received the B.S. and Ph.D. degrees in electrical engineering from Seoul National University, Seoul, South Korea, in 2015 and 2021, respectively.

From 2021 to 2022, he was a Senior Research Engineer with LG Electronics, Seoul. Since 2022, he has been with the Korea Institute of Energy Technology (KENTECH), Naju, South Korea, where he is currently an Assistant Professor. His research interests include grid-connected converter, HVdc/MVdc system, and electric machine drives.

Seung-Ki Sul (Fellow, IEEE) received the B.S., M.S., and Ph.D. degrees in electrical engineering from Seoul National University, Seoul, South Korea, in 1980, 1983, and 1986, respectively.

Since 1991, he has been a Member of the School of Electrical and Computer Engineering, Seoul National University (SNU) faculty. He retired from SNU in August 2023. From September 2023, he has worked for HD Hyundai Group as Technical Advisor in power electronics and electric propulsion of ships. He has authored or coauthored more than 140 IEEE-reviewed journal papers and more than 340 international conference papers in power electronics.

Dr. Sul has been a IEEE Fellow since 2000. In 2015, he was the Korea Institute of Power Electronics President. He was the recipient of the Outstanding Achievement Award from IEEE IAS in 2016 and the William E. Newell Award from IEEE PELS in 2017.